

Original Research

# **Urinary Metabolomics-Driven Discovery of Metabolic Markers and Molecular Subtyping in Liver Cancer**

Hemeng Wu<sup>1,†</sup>, Hongsheng Lin<sup>1,†</sup>, Fuli Long<sup>2</sup>, Rongzhen Zhang<sup>3</sup>, Minpeng Li<sup>4</sup>, Yunyong Wang<sup>1</sup>, Faming Shu<sup>2</sup>, Yangwu Zhang<sup>2</sup>, Mingfen Li<sup>1,\*</sup>, Xiaoling Zhou<sup>2,\*</sup>

Academic Editor: Amancio Carnero Moya

Submitted: 31 July 2025 Revised: 22 September 2025 Accepted: 30 September 2025 Published: 31 October 2025

#### **Abstract**

Background: Primary liver cancer (PLC) exhibits a high incidence and mortality rate. Early diagnosis and effective treatment are crucial for improving patient survival rates. This study aims to identify biomarkers of hepatitis B-related liver cancer and establish a new method for molecular subtype classification based on differential metabolite-related regulatory gene expression profiles. Methods: This study collected sterile midstream urine samples from patients with hepatitis B-related liver cancer who had not received standardized systematic antiviral therapy or anticancer therapy, as well as from healthy controls. Potential biomarkers were identified through liquid chromatography-tandem mass spectrometry (LC-MS/MS)-based metabolomics, followed by Kyoto Encyclopedia of Genes and Genomes (KEGG) enrichment analysis performed on the differential metabolites. Gene expression data of 371 hepatocellular carcinoma (HCC) samples in The Cancer Genome Atlas-Liver Hepatocellular Carcinoma (TCGA-LIHC) database were clustered using gene annotations for differential metabolites derived from the Human Metabolome Database (HMDB). The Kaplan-Meier (KM) survival curve was employed to assess the prognosis of different HCC molecular subtypes. Expression differences of subtype-specific genes and their enrichment in Hallmark, KEGG and Gene Ontology (GO) pathways were analyzed. The Tumor Immune Dysfunction and Exclusion (TIDE) scoring tool was used to evaluate the subtypes' response to immunotherapy. Sensitivity to sorafenib was also compared across the different subtypes. **Result**: A total of 53 differential metabolites were identified (p < 0.01), which were significantly enriched in seven metabolic pathways (p < 0.05). Three potential biomarkers were discovered: Suberic acid, 2'-O-methylcytidine, and 3'-Sialyllactose. Regulatory genes associated with these differential metabolites clustered HCC samples from the TCGA-LIHC database into two molecular subtypes (C1 and C2). KM survival analysis indicated that patients in the C2 subtype exhibited higher overall survival compared to those in C1. Differential genes between the two subtypes were significantly enriched in Hallmark, KEGG and GO pathways. The TIDE scoring tool revealed a higher likelihood of immune escape in C1 subtype patients. Molecular targeted drug analysis suggested that sorafenib may be more effective in patients with the C1 subtype. Conclusions: Suberic acid, 2'-O-methylcytidine, and 3'-Sialyllactose hold promise as metabolic biomarkers for hepatitis B-related liver cancer. Understanding the diversity of the human liver cancer gene expression profile from a metabolomic perspective has potential applications for developing novel clinical treatment strategies.

Keywords: liver neoplasms; urine; metabolomics; biomarkers

## 1. Introduction

Primary liver cancer (PLC) is a common type of cancer, with hepatocellular carcinoma (HCC) being the most prevalent. This condition is marked by high malignancy, subtle onset, and the absence of accurate early diagnosis and treatment indicators [1,2]. The mortality of HCC is high and the 5-year survival rate needs to be improved [3]. Metabolic reprogramming is frequently observed in tumor cells, where significant alterations in metabolic pathways occur to support their rapid growth, survival, and proliferation. HCC is characterized by metabolic reprogramming [4], particularly glucose metabolic reprogramming, which

is fundamental to HCC progression [1]. Hepatitis B virus (HBV) is still the main pathogenic factor of liver cancer in China [5]. Effective and timely screening, diagnosis, and treatment of hepatitis B-related liver cancer are critical components of liver cancer management in China.

Current diagnostic methods for HCC have limitations, and blood samples are commonly used for the detection and exploration of disease biomarkers. Pathology remains the most trusted diagnostic tool for identifying early-stage HCC and its precancerous lesions [6]. Urine, as a non-invasive diagnostic modality, provides greater potential for the investigation of HCC biomarkers [7]. Urine serves as a source of early biomarkers sensitive to physiological changes, re-

<sup>&</sup>lt;sup>1</sup>Department of Clinical Laboratory, The First Affiliated Hospital of Guangxi University of Chinese Medicine, 530023 Nanning, Guangxi, China

<sup>&</sup>lt;sup>2</sup>Department of Hepatology, The First Affiliated Hospital of Guangxi University of Chinese Medicine, 530023 Nanning, Guangxi, China

<sup>&</sup>lt;sup>3</sup>Department of Hepatology, Guangxi International Zhuang Medicine Hospital Affiliated to Guangxi University of Chinese Medicine, 530201 Nanning, Guangxi, China

<sup>&</sup>lt;sup>4</sup>Department of Hepatobiliary Surgery, The First Affiliated Hospital of Guangxi University of Chinese Medicine, 530023 Nanning, Guangxi, China

<sup>\*</sup>Correspondence: limf@gxtcmu.edu.cn (Mingfen Li); zxl\_lz@163.com (Xiaoling Zhou)

<sup>&</sup>lt;sup>†</sup>These authors contributed equally.

flecting subtle and early-stage alterations in body function [8]. Currently, the study of urine metabolites for hepatitis B-related liver cancer remains in the exploratory stage. Studying the changes of its metabolites can understand the metabolic abnormalities of the liver, which is helpful for early diagnosis, screening, monitoring, and prognosis evaluation of the disease. Analyzing the characteristic metabolites in patients' urine provides new insights into the identification of metabolic biomarkers for liver cancer and potential therapeutic targets [9].

This study aims to investigate diagnostic biomarkers and perform subtype analysis of PLC. Using liquid chromatography-tandem mass spectrometry (LC-MS/MS)-based untargeted metabolomics, we analyzed the metabolic profiles of urine metabolites in patients with hepatitis B-related liver cancer and healthy controls. Our objective is to identify potential metabolic biomarkers with high sensitivity and specificity for hepatitis B-related liver cancer, as well as to explore the characteristics of different HCC subtypes from the perspective of urinary metabolites. This study hopes to bring new insights into the non-invasive diagnosis and molecular characteristics of PLC.

### 2. Materials and Methods

### 2.1 Study Subjects

This study collected urine samples from 10 patients with hepatitis B-related liver cancer and 8 healthy controls. The inclusion criteria for patients were as follows: (1) patients with a clinical diagnosis of PLC, with a confirmed history of HBV infection. Currently, both Hepatitis B Surface Antigen (HBsAg) and HBV DNA are positive, with HBsAg and/or HBV DNA positivity persisting for more than 6 months. (2) These patients have not received standardized and systematic antiviral therapy for HBV, nor have they undergone antitumor treatments such as surgery, radiotherapy, chemotherapy, or immunotherapy. The inclusion criteria of the healthy control group are as follows: (1) subjects had no history of HBV infection, hypertension, diabetes, or other relevant conditions; (2) liver function and alpha-fetoprotein (AFP) results were within normal limits; (3) ultrasound examination confirmed no significant abnormalities in the liver, kidneys, and pancreas. Exclusion criteria are as follows: (1) subjects with chronic liver diseases of other etiologies, including drug-induced liver disease, alcoholic liver disease, non-alcoholic fatty liver disease, autoimmune liver disease, and metabolic liver disease; (2) subjects with secondary liver cancer, other malignancies or severe kidney disease. Two sets of routine test results were collected, with AFP measured using the Abbott ARCHI-TECT i2000SR system (Abbott Laboratories, Chicago, IL, USA) and routine biochemical assays conducted using the Abbott ARCHITECT c16000 system (Abbott Laboratories, Chicago, IL, USA).

#### 2.2 Sample Processing and Extraction

Midstream urine samples were aseptically collected from all participants, followed by centrifugation at 3000 rpm for 10 min at 4 °C. The resulting supernatant was aliquoted into cryovials and stored at –80 °C until analysis. For quality control, a pooled sample was created by combining equal volumes of urine from each individual.

Following collection, the urine samples were thawed at 4 °C. An aliquot of each sample was then transferred into a pre-cooled solution of methanol (catalog number A456-4, Fisher Scientific, Waltham, MA, USA)/acetonitrile (catalog number 1499230-935, Merck KGaA, Darmstadt, Hesse, Germany)/water (catalog number W6-4, Fisher Scientific, Waltham, MA, USA) (2:2:1, v/v). After thorough vortexing, the mixtures were sonicated at low temperature for 30 min. The sample was kept under frozen conditions (–20 °C) for 10 min, followed by low-temperature high-speed centrifugation at 14,000 g for 20 min at 4 °C. The supernatant was then vacuum-dried.

The vacuum-dried samples were reconstituted in 100  $\mu$ L acetonitrile/water (1:1, v/v) solvent. The mixtures were then centrifuged at 14,000 g for 15 min at 4 °C. Finally, the supernatant was analyzed by mass spectrometry.

### 2.3 Metabolomics Detection and Data Analysis

Throughout the analytical process, all samples were maintained at 4 °C in the autosampler for continuous analysis in a random order. Analysis was performed using a UHPLC (Agilent 1290 Infinity LC, Agilent Technologies, Santa Clara, CA, USA) equipped with a HILIC column (ACQUITY UPLC BEH Amide, Waters Corporation, Milford, MA, USA) and coupled to a quadrupole time-of-flight (AB Sciex TripleTOF 6600, AB Sciex Pte. Ltd., Framingham, MA, USA). The column temperature was maintained at 25 °C. The mobile phase consisted of A = 25 mM ammonium acetate (catalog number 73594, Sigma-Aldrich, St. Louis, MO, USA) and 25 mM ammonium hydroxide (catalog number A470-500, Fisher Scientific, Waltham, MA, USA) in water, and B = acetonitrile. A constant flow rate of 0.5 mL/min was applied, and the injection volume was 2 μL.

Raw data files were converted into MzML format using ProteoWizard (version 3.0.6428, https://proteowizard.sourceforge.io/), and then processed using the XCMS online (version 3.7.1, https://xcmsonline.scripps.edu/) program for peak alignment, retention time correction, and peak area extraction. The molecular feature peaks of the samples were annotated with metabolites by referencing public databases such as Mass Bank (https://massbank.eu/MassBank/), Metlin (https://metlin.scripps.edu/), and MoNA (https://mona.fiehnlab.ucdavis.edu/), in conjunction with a secondary mass spectrometry database. To establish gene-metabolite associations, we queried the Human Metabolome Database (HMDB, https://hmdb.ca) and restricted the analysis to high-confidence pairs with ex-



Table 1. Clinical characteristics of healthy controls and patients.

Variables	Healthy controls $(n = 8)$	Ca $(n = 10)$	<i>p</i> -value
Age (years)	$51.00 \pm 4.66$	$55.50 \pm 11.22$	0.271
Male/female	4/4	7/3	0.630*
AFP (ng/mL)	3.13 (2.09~3.57)	607.49 (14.94~1200.00)	0.002
TP (g/L)	$71.30 \pm 2.98$	$66.78 \pm 4.70$	0.031
ALB (g/L)	$44.66 \pm 2.25$	$35.58 \pm 6.07$	0.001
TBIL ( $\mu$ mol/L)	15.70 (11.85~19.58)	17.55 (12.70~21.60)	0.307
DBIL (µmol/L)	4.30 (3.38~4.50)	6.10 (4.08~7.40)	0.029
ALT (U/L)	7.50 (5.25~13.00)	53.50 (47.75~88.00)	0.001
AST (U/L)	$16.50 \pm 4.17$	$75.70 \pm 40.48$	0.001
GGT (U/L)	15.50 (12.00~23.25)	172.50 (72.50~310.00)	0.001

<sup>\*,</sup> Categorical variables were analyzed using Fisher's exact test. Quantitative variables were first assessed for normality; if normally distributed, the data were expressed as mean  $\pm$  SD. If the data were not normally distributed, they were expressed as M (P25–P75). Abbreviations: AFP, alpha-fetoprotein; TP, total protein; ALB, albumin; TBIL, total bilirubin; DBIL, direct bilirubin; ALT, alanine aminotransferase; AST, aspartate aminotransferase; GGT, gamma-glutamyl transferase.

plicit experimental evidence (e.g., enzyme- or transporterrelated), supported by *in vitro*, clinical, or validated bioinformatic studies.

#### 2.4 Statistical Analysis

Clinical data were analyzed using SPSS26.0 (IBM Corp., Armonk, NY, USA). For categorical variables, intergroup comparisons were conducted using Fisher's exact test. The quantitative variables were first assessed for normality, and then analyzed using parametric or non-parametric tests, as appropriate. Metabolomics data were analyzed using R packages, such as pheatmap (version 1.0.12, https://cran.r-project.org/web/packages/pheatmap/index.html), gmodels (version 2.18.1, https://cran.r-project.org/web/packages/gmodels/index.html), ropls (version 1.7.2, https://bioconductor.org/packages/release/bioc/html/ropls.html), and pROC (version 1.15.3, https://cran.r-project.org/web/packages/pROC/), among others. Molecular subtyping analysis was performed using R software (version 4.0.3, https://www.r-project.org/).

### 3. Results

### 3.1 Characteristics of the Study Population

Table 1 presents the basic clinical data of the healthy population and patients with hepatitis B-related liver cancer. The results indicate that there were no statistically significant differences in age and gender between the two groups (p > 0.05). Compared to the healthy population, the liver cancer group exhibited significantly elevated levels of AFP, direct bilirubin (DBIL), alanine aminotransferase (ALT), aspartate aminotransferase (AST), and gammaglutamyl transferase (GGT), while total protein (TP) and albumin (ALB) levels were significantly decreased (p < 0.05).

# 3.2 Construction and Validation of Urine Model Based on PCA and OPLS-DA

On the principal component analysis (PCA) plot, the quality control samples were densely distributed, with significant differences between the two groups and good repeatability within each group (Fig. 1A,B). The orthogonal partial least square discriminant analysis (OPLS-DA) score plot indicated R2X = 0.213, R2Y = 0.962, and Q2Y = 0.556, demonstrating that the established model has a good predictive ability (Fig. 1C). The permutation test plot confirmed the reliability of the OPLS-DA model (Fig. 1D).

# 3.3 Screening of Differential Metabolites in Urine and KEGG Enrichment Analysis

The criteria for screening differential metabolites in this study were as follows: variable importance in the projection (VIP)  $\geq 1$  in the OPLS-DA model and p < 0.01in the t-test. A total of 53 differential metabolites were identified, including 44 significantly upregulated and 9 significantly downregulated metabolites. Among them, 36 metabolites were annotated in the HMDB and classified accordingly (Fig. 2A). A volcano plot was utilized to illustrate the expression levels of differential metabolites between the groups (Fig. 2B). VIP plots show the importance of metabolites and their contribution to sample discrimination (Fig. 2C). The Z-score plot of differential metabolites (MS2 level) was employed to assess the relative content of metabolites at the same level (Fig. 2D). Table 2 lists the top 20 differential metabolites based on VIP values, where a higher VIP value indicates a greater contribution of the metabolite in distinguishing between the compared groups.

A Kyoto Encyclopedia of Genes and Genomes (KEGG) enrichment analysis was performed on the 53 differential metabolites between the comparison groups, identifying 35 enriched metabolic pathways. A bub-



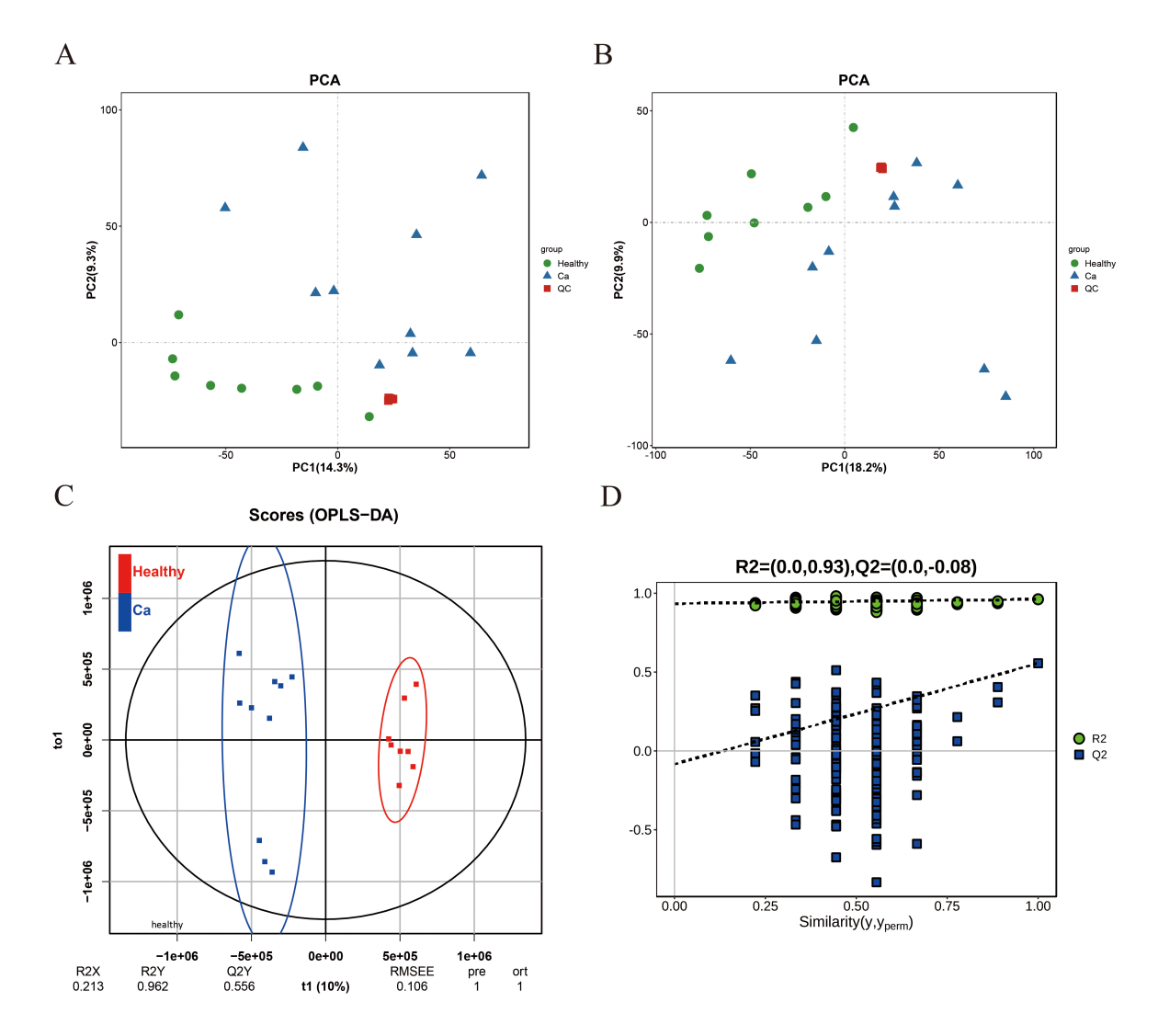


Fig. 1. PCA and OPLS-DA urinary models distinguish populations between the comparison groups. (A,B) PCA model plot in positive and negative ion mode. (C) OPLS-DA model score plot. (D) OPLS-DA model permutation test plot. PCA, principal component analysis; OPLS-DA, orthogonal partial least square discriminant analysis.

ble plot of the top 15 significantly enriched pathways was generated based on the p-values (Fig. 2E). Additionally, an enrichment circle plot was generated to illustrate the significance of the top 15 metabolic pathways based on p-values, as well as the number of upregulated and downregulated metabolites, and the metabolites ratio (Fig. 2F). Seven metabolic pathways exhibited significant differences (p < 0.05), including the pantothenate and CoA biosynthesis, 2-oxocarboxylic acid metabolism, butanoate metabolism, cyanoamino acid metabolism, microbial metabolism in diverse environments, nicotinate and nicotinamide metabolism, glycine, serine and threonine metabolism.

# 3.4 Metabolomics-Based Potential Urinary Biomarkers for Hepatitis B-Related Liver Cancer

In this study, receiver operating characteristic (ROC) curve analysis was employed to assess the performance

of the selected differential metabolites by calculating their area under the curve (AUC) values (Fig. 3). A ten-fold cross-validation was conducted, and the mean AUC values were computed to reduce the risk of model overfitting. The results revealed that the AUC mean values of three differential metabolites were greater than 0.9, namely Suberic acid, 2'-O-methylcytidine, and 3'-Sialyllactose. Specifically, Suberic acid AUC = 1 (healthy controls, n = 8; liver cancer, n = 10; 95% CI:  $1.000 \sim 1.000$ ). 2'-O-methylcytidine AUC = 0.975 (95% CI:  $0.930 \sim 0.945$ ). 3'-Sialyllactose AUC = 0.938 (95% CI:  $0.942 \sim 0.956$ ). Table 3 provides detailed information on these three potential metabolic markers.

# 3.5 Identification and Prognostic Analysis of Molecular Subtypes of HCC

By querying the HMDB database, we identified 53 differentially expressed metabolites and retrieved their an-



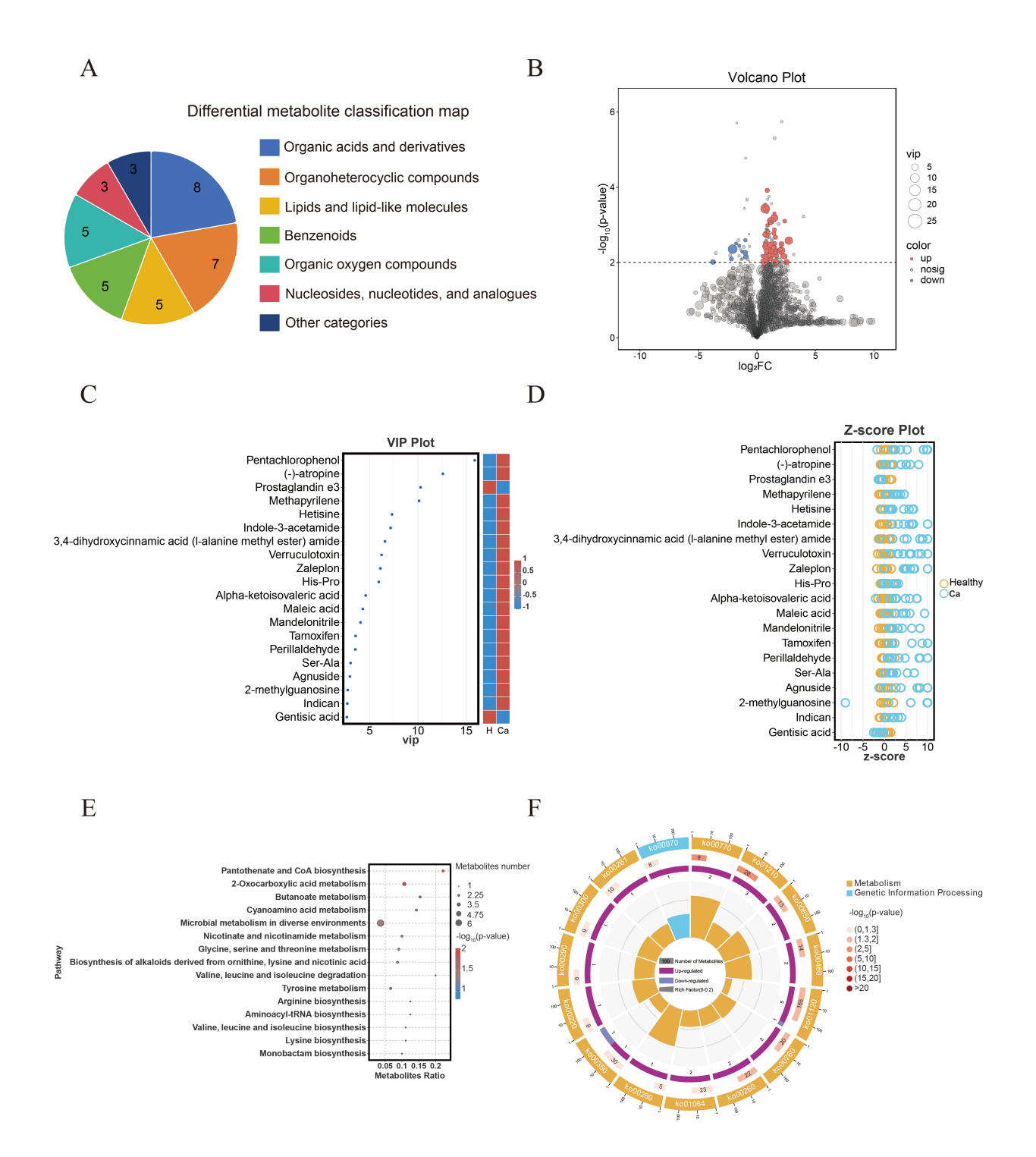


Fig. 2. Differential metabolites in urine between different groups exhibit distinct characteristics. (A) Classification map of differential metabolites. (B) Volcano plot of differential metabolites. (C) VIP plot of differential metabolites. (D) Z-score plot of differential metabolites. (E) KEGG enrichment bubble plot of differential metabolites. The size of the circle represents the number of differential metabolites enriched in each pathway. (F) Metabolic pathway circle plot. VIP, variable importance in the projection; KEGG, Kyoto Encyclopedia of Genes and Genomes.

notated gene information. This resulted in a final set of 98 metabolite-related regulatory genes, including enzymes and proteins. The metabolic regulatory genes were then subjected to consistent clustering with gene expression data

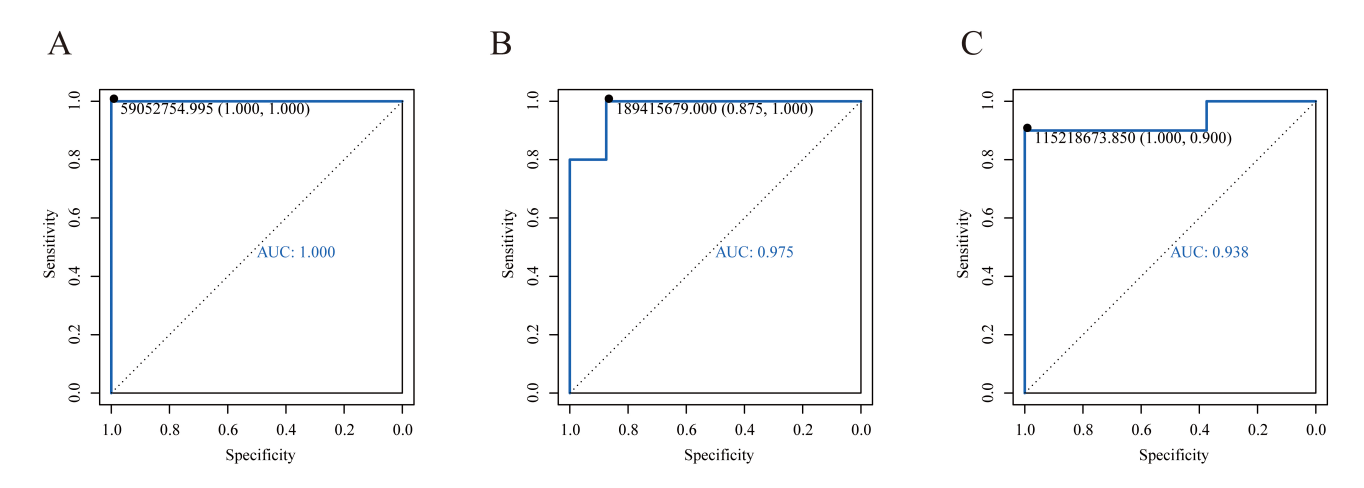
from 371 HCC samples in The Cancer Genome Atlas-Liver Hepatocellular Carcinoma (TCGA-LIHC) database. When K=2, two stable clusters were generated, and the matrix heatmap divided HCC into two molecular subtypes, C1 and



Table 2. The top 20 differential metabolites of VIP value.

Metabolite	log <sub>2</sub> FC	<i>p</i> -value	VIP	RT	m/z
Pentachlorophenol	1.319670893	0.005193234	15.87797916	0.753	263.02308
(-)-atropine	1.300709850	0.004324274	12.58696117	6.976	290.15969
Prostaglandin e3	-2.085074706	0.004407285	10.26758020	3.643	331.17628
Methapyrilene	0.697147177	0.000366731	10.11932463	7.049	262.12846
Hetisine	0.805211339	0.003716509	7.318897691	4.097	330.22736
Indole-3-acetamide	2.716237334	0.002617423	7.177248219	7.002	175.07133
3,4-dihydroxycinnamic acid (l-alanine methyl ester) amide	2.072153586	0.004808742	6.590770361	0.888	232.05928
Verruculotoxin	1.486965976	0.000645205	6.241679989	4.050	243.13503
Zaleplon	1.178122656	0.000781359	6.119466205	7.008	264.11886
His-Pro	0.620611090	0.009466142	5.952839278	2.584	235.11890
Alpha-ketoisovaleric acid	0.860165726	0.006610992	4.601905686	2.242	115.04007
Maleic acid	0.778322529	0.001799395	4.303796919	0.871	115.00370
Mandelonitrile	1.160697155	0.003412904	4.065987293	1.053	134.08119
Tamoxifen	2.527436553	0.009707497	3.553467422	5.745	372.23808
Perillaldehyde	2.289121455	0.006801001	3.534889206	3.409	169.13351
Ser-Ala	1.640677069	0.009690771	3.039145470	2.988	177.06581
Agnuside	2.091059830	0.003236282	2.967104677	0.882	465.12568
2-methylguanosine	1.123081135	0.007675389	2.739367426	3.601	296.10004
Indican	0.811175486	0.004991964	2.694630637	1.207	296.13521
Gentisic acid	-0.945866373	0.007011832	2.647569997	1.771	153.01932

RT, retention time; VIP, variable importance in the projection.



**Fig. 3. ROC curves of potential biomarkers.** (A) ROC curve of Suberic acid. (B) ROC curve of 2'-O-methylcytidine. (C) ROC curve of 3'-Sialyllactose. ROC, receiver operating characteristic.

C2 (Fig. 4A). The results revealed significant differences in the expression of metabolic regulatory genes between the two molecular subtypes. Kaplan-Meier (KM) analysis indicated a statistically significant difference in overall survival between the subtypes (Fig. 4B, p < 0.05). Patients with the C2 had significantly longer survival times and a more favorable prognosis than those in the C1 subtype (p < 0.05).

As shown in Table 4, significant differences in clinicopathological characteristics were observed between the C1 and C2 subtypes. Specifically, the C1 subtype demonstrated more aggressive features, including a significantly higher proportion of high-grade (G3/G4) tumors (p <

0.001) and a more advanced T stage (p = 0.005). Consequently, the clinical stage was significantly more advanced in the C1 group (p = 0.001). This aggressive profile was associated with a poorer clinical prognosis, reflected by a significantly higher mortality rate in the C1 subtype (p = 0.01).

# 3.6 Pronounced Differences in Genes Expression Across HCC Molecular Subtypes

Differentially expressed genes between the two subtypes were selected based on  $|\log_2 \text{FoldChange}| > 1$  and p < 0.05. A volcano plot (Fig. 5A) was used to illustrate the differential genes between C1 and C2. The re-



Table 3. Related information of potential metabolic markers.

Metabolite	AUC	AUC Mean $\pm$ SD	Specificity	Sensitivity	Class	HMDB	<i>p</i> -value
Suberic acid	1	$1 \pm 0.000$	1	1	Fatty Acyls	HMDB0000893	0.004540413
2'-O-methylcytidine	0.975	$0.938 \pm 0.165$	0.875	1	Pyrimidine nucleosides	HMDB0242132	0.000120391
3'-Sialyllactose	0.938	$0.949 \pm 0.151$	1	0.900	Organooxygen compounds	HMDB0000825	0.000445886

AUC, area under the curve; HMDB, Human Metabolome Database.

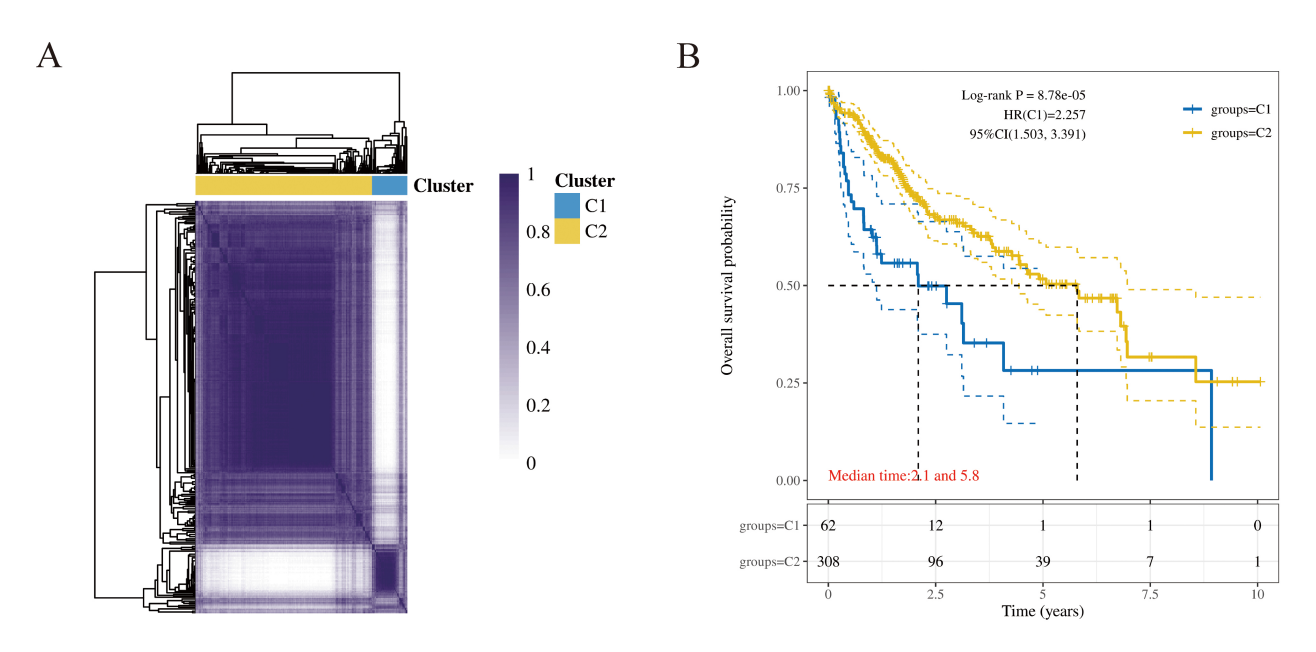


Fig. 4. Construction and prognosis analysis of molecular subtypes in HCC. (A) Consensus matrix heatmap of molecular subtypes. When K = 2 is the optimal number of clusters. (B) KM survival curve of molecular subtype. Patients in the C1 subtype had significantly shorter overall survival than those in the C2 subtype (log-rank test, p < 0.05). HCC, hepatocellular carcinoma; KM, Kaplan-Meier.

sults revealed that 1894 genes, including CA9, KRT19, and DOK1, were upregulated, while 438 genes, including HPR, APOC3, and RTP3, were downregulated. A clustering heatmap was utilized to illustrate the differential expression of metabolism-related regulatory genes between the transcriptomic results of the C1 and C2 HCC molecular subtypes (Fig. 5B). Enrichment analysis using the Hallmark gene set revealed significant differences between the molecular subtypes in core pathways, such as the cell cycle and metabolic reprogramming (Fig. 5C). KEGG enrichment analysis highlighted potential signaling pathways involved (Fig. 5D). Gene Ontology (GO) enrichment analysis provided insights into the primary molecular functions (MF), cellular components (CC), and biological processes (BP) associated with the differential genes between the two molecular subtypes (Fig. 5E-G). These findings indicate that the subtype-specific genes are significantly enriched in Hallmark, KEGG, and GO pathways.

# 3.7 Differential Sensitivity to Immune Therapy and Targeted Therapy in HCC Molecular Subtypes

The Tumor Immune Dysfunction and Exclusion (TIDE, http://tide.dfci.harvard.edu/) scoring tool was utilized to evaluate the potential for immune evasion in the two HCC molecular subtypes, derived from signatures of T-

cell dysfunction and T-cell exclusion scores. Compared to the C2 subtype, the C1 subtype demonstrated significantly higher TIDE, Exclusion, and myeloid-derived suppressor cell (MDSC) scores, alongside a lower microsatellite instability (MSI) score (Fig. 6A–E). These results indicate that the C1 subtype is associated with a higher risk of immune evasion, potentially due to the presence of a greater number of immunosuppressive cells. Conversely, the C2 subtype, characterized by higher MSI, showed increased sensitivity to immunotherapy, suggesting a higher likelihood of clinical benefit. Consequently, the C2 subtype is associated with a more favorable prognosis, a conclusion supported by our KM survival analysis.

This study analyzed the transcriptomic data of HCC samples from different molecular subtypes using the Genomics of Drug Sensitivity in Cancer (GDSC, https://www.cancerrxgene.org/) database (Fig. 6F, p < 0.05). The results indicate that the half maximal inhibitory concentration (IC $_{50}$ ) of sorafenib was lower in patients of C1 subtype compared to those in the C2 subtype, suggesting that sorafenib may exhibit enhanced efficacy in C1 subtype patients (p < 0.05). These findings imply that the sensitivity of HCC patients to targeted anti-tumor therapies may differ across molecular subtypes.



Table 4. Comparison of clinical and pathological characteristics between subtypes C1 and C2.

Living conditions         Alive Dead         31 by 99         0.010           Age         Mean ± SD         59.1 ± 12.8         59.5 ± 13.7         0.820           Gender         Female Male         26 by 214         95         0.117           Age         Male         36 by 214         214         214           Age         American Indian Male         1         1         1         2         2         0.117         2         0.266         2         0.117         0.266         2         0.266         2         0.266         2         0.266         2         0.266         2         0.266         2         0.266         2         0.266         2         0.266         2         0.266         2         0.266         2         0.266         2         0.266         2         0.266         <	Item	Characteristics	C1	C2	<i>p</i> -value	
Age         Mean ± SD         59.1 ± 12.8         59.5 ± 13.7         0.820           Gender         Female Male         26         95 male         0.117           Race         American Indian Asian 31 127 male         0.266         0.266         0.266           Black 1 16 male         1 16 male         165 male         0.266           Black 1 1 6 male         1 16 male         165 male           T2 20 72 male         72 male         72 male           T2a 1 male         1 male         - male           T2a 1 male         - male         - male           T3a 13 32 0.005         0.005           T3a 6 23 male         2 male           T4 3 male         3 male           N stage         N1 2 male         2 male           N stage         N1 2 male         2 male           M stage         MX 13 male         88 male           M stage         MX 13 male         88 male           III 19 male         67 male         67 male           III 19 male         67 male         60 male           III 1 male	T 1 1 11/1	Alive	31	210	0.010	
Gender         Female Male         26 male         95 male         0.117           American Indian         1         1         1           Asian         31         127 mark         0.266           Black         1         16 mark         16 mark           White         29         155         15           T1         16 mark         165 mark         16 mark         16 mark           T2         20 mark         72 mark         73 mark         74 mark </td <td>Living conditions</td> <td>Dead</td> <td>31</td> <td>99</td>	Living conditions	Dead	31	99		
Gender         Male         36         214         0.117           Race         American Indian         1         1         1           Black         1         16         16         0.266           Black         1         16         165         15         15         16         165         15         16	Age	Mean $\pm$ SD	$59.1 \pm 12.8$	$59.5 \pm 13.7$	0.820	
Male         36         214           American Indian         1         1           Asian         31         127           Black         1         16           White         29         155           T1         16         165           T2         20         72           T2a         1         -           T2b         1         -           T3a         13         32         0.005           T3a         6         23           T3b         2         4         4           T4         3         10         10           TX         -         1         1           N stage         N1         2         2         0.148           M         16         98         0.266           MX         13         88         0.266           MI         -         4         -           III         19         67         1           III         -         3         1           IIII         -         3         1           IIII         -         3         0.001	Candan	Female	26	95	0.117	
Race       Asian Black Black Dwhite       1 16 16 165 155       0.266         T1 Hold White       29 155       155         T1 Hold Hold Black T2 20 72 T2 T2a 1 — T2b 1 — T2b 1 — T2b 1 — T2b 1 — T3a 66 23 T3b 2 4 T4 33 10 TX — 1       2 4 T4 33 10 TX — T4 T4 T4 T4 T5 T5 T56 T56	Gender	Male	36	214	0.117	
Black   1		American Indian	1	1		
Black   1	Race				0.266	
T1 16 165 T2 20 72 T2a 1 - T2b 1 - T2b 1 - T2b 1 - T2b 1 32 0.005 T3a 6 23 T3b 2 4 T4 3 10 TX - 1  N0 43 209 N stage N1 2 2 0.148 NX 16 98  M0 49 217 M stage MX 13 88 0.266 M1 - 4  I 15 156 II 19 67 III - 3 IIIA 17 48 Clinical stage IIIB 2 6 0.001 IIIC 4 5 IV - 2 IVA - 1 IVB - 2 Tumor grade G2 23 154 G3 33 89 <0.001	Race	Black	1	16	0.200	
T2 20 72 T2a 1 - T2b 1		White	29	155		
T stage  T2a T2b 1 - T3a 32 0.005  T3a 6 23 T3b 2 4 T4 3 10 TX - 1  N0 43 209 Nstage N1 2 2 2 0.148 NX 16 98  M0 49 217 Mstage MX 13 88 0.266 M1 - 4  III 19 67 III 19 67 III - 3 IIIA 17 48  Clinical stage IIIB 2 6 0.001 IIIC 4 5 IV - 1 VA - IVA - IVA - IVA - IVA - IVA - IVB -  Tumor grade  G3 33 89  <  Tumor grade  Tumor grade  Table 1 - Ta		T1	16	165		
T stage  T2b  T3  T3  T3  T3a  6  23  T3b  2 4  T4  3 10  TX  - 1  N0  A3  N0  A43  N0  A43  N0  A43  N0  A43  N0  A43  N0  A43  A43  N0  A44  NX  A44  NX  A44  A44  A44  A44		T2	20	72		
T stage		T2a	1	_		
T3a 6 23 T3b 2 4 T4 3 10 TX - 1  N0 43 209 N stage N1 2 2 2 0.148 NX 16 98  M0 49 217 M stage MX 13 88 0.266 M1 - 4  I 15 156 II 19 67 III - 3 IIIA 17 48 Clinical stage IIIB 2 6 0.001 IIIC 4 5 IV - 2 IVA - 1 IVB - 2  Tumor grade G3 33 89  Clinical stage G3 33 89  Tumor grade C3 53 Tumor grade C5 C3		T2b	1	_		
T3b 2 4 T4 3 10 TX - 1  N0 43 209 N stage N1 2 2 2 0.148 NX 16 98  M0 49 217 M stage MX 13 88 0.266 M1 - 4  I 15 156 II 19 67 III - 3 IIIA 17 48  Clinical stage IIIB 2 6 0.001 IIIC 4 5 IV - 2 IVA - 1 IVB - 2  Tumor grade G2 23 154 G3 33 89 <0.001	T stage	Т3	13	32	0.005	
T4 3 10 TX - 1  N0 43 209 N stage N1 2 2 0.148 NX 16 98  M0 49 217 M stage MX 13 88 0.266 M1 - 4  I 15 156 III 19 67 III - 3 IIIA 17 48  Clinical stage IIIB 2 6 0.001 IIIC 4 5 IV - 2 IVA - 1 IVB - 2  Tumor grade G3 33 89 <0.001		T3a	6	23		
TX       −       1         N0       43       209         N stage       N1       2       2       0.148         MX       16       98         M0       49       217         M stage       MX       13       88       0.266         M1       −       4       4         II       15       156       156         III       −       3       111       −       3         IIIA       17       48       0.001       111       −       3       111       −       2       6       0.001       <		T3b	2	4		
N stage  N0 43 209 N1 2 2 0.148 NX 16 98  M0 49 217 M stage  MX 13 88 0.266 M1 - 4  I 15 156 II 19 67 III - 3 IIIA 17 48  Clinical stage  IIIB 2 6 IV - 2 IVA - IVB - 1 IVB - 2  Tumor grade  G2 23 154 G3 33 89		T4	3	10		
N stage N1 2 2 0.148  NX 16 98  M0 49 217  M stage MX 13 88 0.266  M1 - 4  I 15 156  II 19 67  III - 3  IIIA 17 48  Clinical stage IIIB 2 6 0.001  IIIC 4 5  IV - 2  IVA - 1  IVB - 2  Tumor grade G2 23 154  G3 33 89 <0.001		TX	_	1		
NX 16 98  M0 49 217  M stage MX 13 88 0.266  M1 - 4  I 15 156  II 19 67  III - 3  IIIA 17 48  Clinical stage IIIB 2 6 0.001  IIIC 4 5  IV - 2  IVA - 1  IVB - 2  Tumor grade G3 33 89 <0.001		N0	43	209		
Mo 49 217  Mx 13 88 0.266  M1 - 4  I 15 156  II 19 67  III - 3  IIIA 17 48  Clinical stage IIIB 2 6 0.001  IIIC 4 5  IV - 2  IVA - 1  IVB - 2  Tumor grade G2 23 154  G3 33 89 <0.266	N stage	N1	2	2	0.148	
M stage MX 13 88 0.266 M1 - 4  I 15 156 II 19 67 III - 3 IIIA 17 48  Clinical stage IIIB 2 6 0.001 IIIC 4 5 IV - 2 IVA - 1 IVB - 2  Tumor grade G2 23 154 G3 33 89 <0.266		NX	16	98		
$ \begin{array}{c ccccccccccccccccccccccccccccccccccc$		M0	49	217		
$\begin{array}{c ccccccccccccccccccccccccccccccccccc$	M stage	MX	13	88	0.266	
$\begin{array}{c ccccccccccccccccccccccccccccccccccc$		M1	_	4		
$\begin{array}{c ccccccccccccccccccccccccccccccccccc$		I	15	156		
$\begin{array}{c ccccccccccccccccccccccccccccccccccc$		II	19	67		
Clinical stage IIIB 2 6 0.001 IIIC 4 5 IV - 2 IVA - 1 IVB - 2  G1 2 53 G2 23 154 G3 33 89 <0.001		III	_	3		
$\begin{array}{c ccccccccccccccccccccccccccccccccccc$		IIIA	17	48		
$\begin{array}{c ccccccccccccccccccccccccccccccccccc$	Clinical stage	IIIB	2	6	0.001	
$\begin{array}{c ccccccccccccccccccccccccccccccccccc$		IIIC	4	5		
$\begin{array}{c ccccccccccccccccccccccccccccccccccc$		IV	_	2		
$\begin{array}{cccccccccccccccccccccccccccccccccccc$		IVA	_	1		
Tumor grade $\begin{array}{cccc} G2 & 23 & 154 \\ G3 & 33 & 89 \end{array} < 0.001$		IVB	_	2		
Tumor grade G3 33 89 <0.001		G1	2	53		
G3 33 89	Tumon and 1-	G2	23	154	<0.001	
G4 3 9	rumoi grade	G3	33		< 0.001	
		G4	3	9		

### 4. Discussion

The global mortality rate of hepatitis B-related liver disease is high, and the burden of PLC remains heavy. The early diagnosis and effective treatment of HCC are critical areas of focus, but they remain challenging. Traditional treatments often result in resistance and/or a high rate of recurrence [10,11], as well as other challenges, including tumor heterogeneity, the immunosuppressive tumor microenvironment, and the lack of effective biomarkers. HCC is the only solid tumor that can be diagnosed based on imaging and epidemiological data without the need for pathological confirmation [12]. Accurate diagnosis and personalized treatment of PLC are crucial, as they facilitate early

intervention. This approach is key to improving therapeutic efficacy, optimizing treatment regimens, and ultimately enhancing patient survival rates.

This study revealed significant differences in urinary metabolites between healthy individuals and patients with hepatitis B-related liver cancer. Understanding the patterns of these urinary metabolite changes could facilitate disease identification and diagnosis. The non-invasive diagnosis using urinary biomarkers holds significant application value in evaluating and determining an individual's metabolic functional status [13]. Our research indicates that Suberic acid, 2'-O-methylcytidine, and 3'-Sialyllactose in urine potential as non-invasive urinary biomarkers for hepatitis B-related liver cancer. However, the study based on



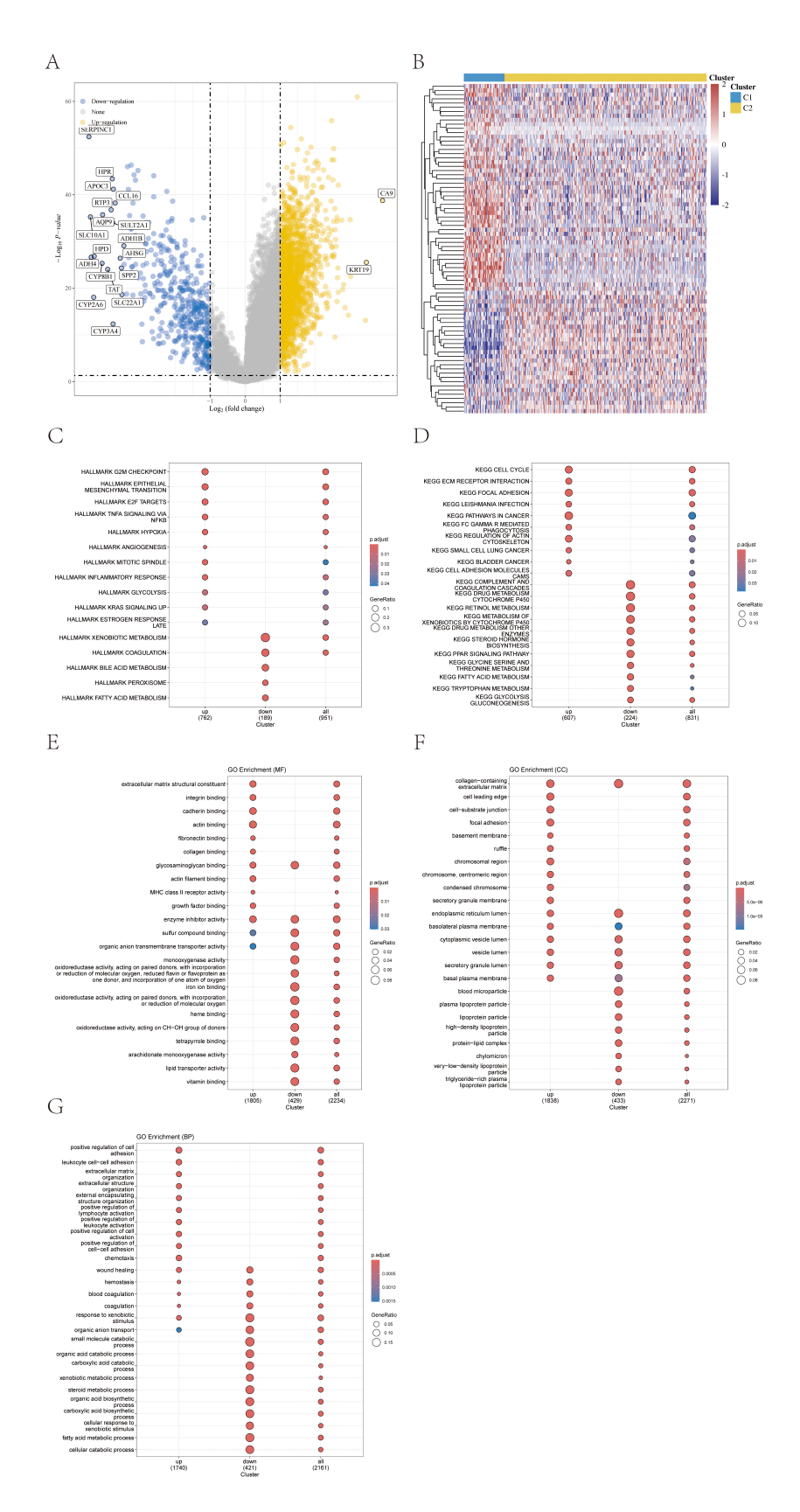


**Fig. 5.** Analysis of gene expression differences between molecular subtypes. (A) Volcano plot of differentially expressed genes between C1 and C2 subtypes. (B) Clustering heatmap of differential metabolites. (C–G) Hallmark, KEGG, GO gene enrichment dotplot. KEGG, Kyoto Encyclopedia of Genes and Genomes; GO, Gene Ontology.

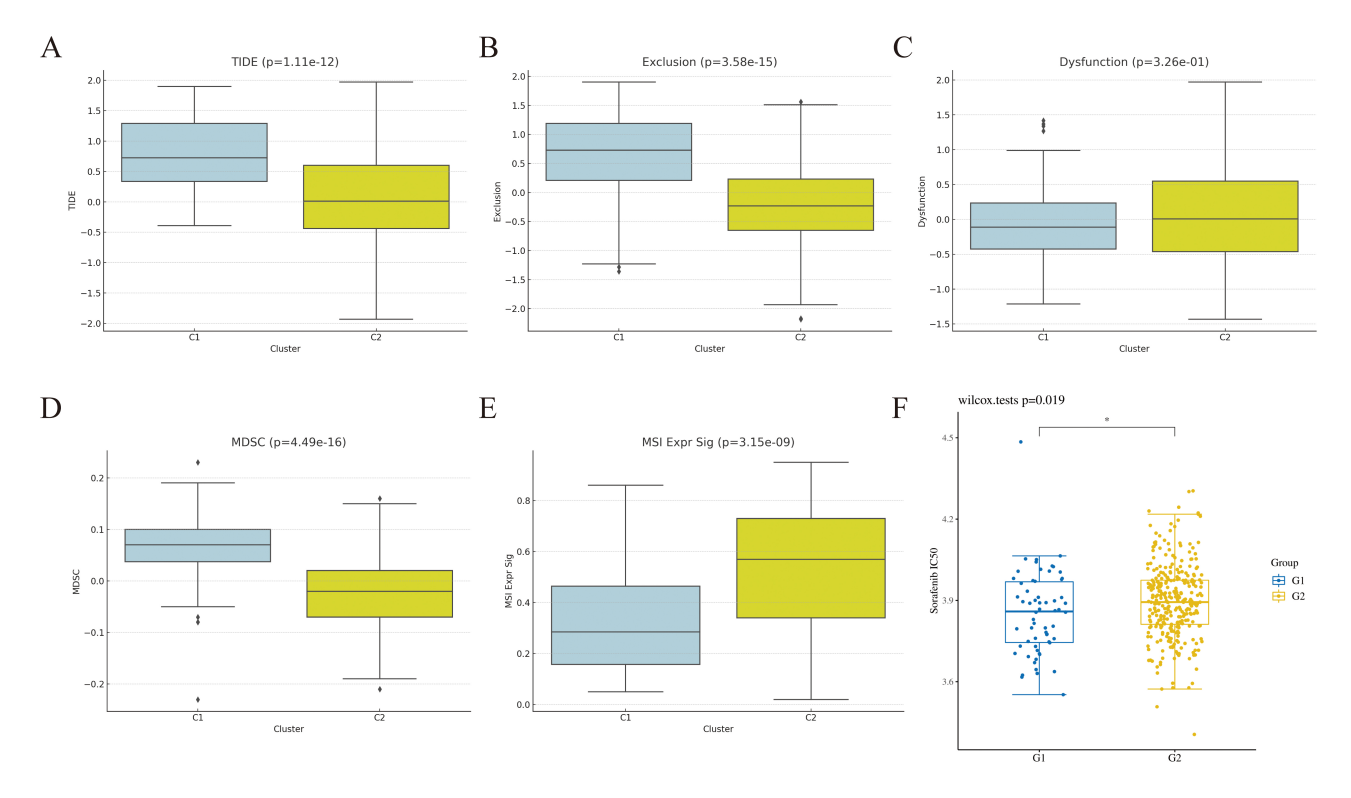


**Fig. 6. Treatment prediction of molecular subtypes.** (A) TIDE, Tumor Immune Dysfunction and Exclusion. (B) Exclusion. (C) Dysfunction. (D) MDSC, myeloid-derived suppressor cell. (E) MSI, microsatellite instability. (F) Drug sensitivity analysis of sorafenib. The scatter points represent individual patients from different subtypes. G1 represents the C1 subtype, and G2 represents the C2 subtype, p = 0.019. \* p < 0.05. The diamond symbols denote outlier samples.

a relatively small size has inherent limitations and may be subject to optimism bias. We performed ten-fold cross-validation with k=10 and times =200, which aims to minimize this bias, although this constitutes internal validation only. In future studies, we plan to incorporate an external validation cohort to further verify these findings by expanding the sample size, refining disease classifications, and conducting stratified analyses, while also assessing the stability of these biomarkers.

Suberic acid is not only synthesized by plants but also generated endogenously within the human body [14]. During the development of HCC, alterations in the levels of suberic acid may be closely associated with mitochondrial dysfunction and disturbances in fatty acid metabolism. Cancer cells exhibit aberrant fatty acid metabolism, which may lead to altered accumulation of certain metabolic intermediates, such as suberic acid. Tumor-derived extracellular vesicles and particle-associated fatty acid cargo promote liver inflammation and the development of fatty liver [15]. Dysregulation of lipid metabolism, a central feature of liver cancer, promotes tumor growth and survival, while pro-protein convertase subtilisin/kexin type 9 (PCSK9) inhibition induces excessive lipid accumulation, thereby enhancing cancer cell susceptibility to ferroptosis [16]. 2'-O-methylcytidine, as a modified nucleotide, plays a crucial role as an epigenetic marker, particularly in the devel-

opment of tumors and cancer. Extensive dysregulation of intracellular RNA modifications may influence the translation efficiency of oncogenes or tumor suppressor genes, thereby contributing to the pathogenesis of liver cancer. In hepatitis B-related liver cancer, the replication of the virus and the expression of its genes may be regulated by RNA modification mechanisms. 2'-O-methylcytidine is an effective inhibitor of hepatitis C virus (HCV) RNA replication [17]. Its levels are significantly reduced in the serum [18] and early urine samples [19] of breast cancer patients, while they are elevated in colorectal cancer organoids, particularly in response to 5-fluorouracil treatment [20]. Research has revealed notable differences in the levels of 2'-O-methylcytidine between cancerous and non-cancerous tissues [21]. 3'-Sialyllactose is an important human milk oligosaccharide with significant immunomodulatory effects [22], and it exhibits specific physiological and biochemical functions across various tissues. It has been shown to alleviate inflammation and reduce the development of atherosclerosis [23], as well as provide protective effects against lipopolysaccharide (LPS)-induced lung injury [24]. The liver is a major site for 3'-Sialyllactose distribution and metabolism [25]. 3'-Sialyllactose, in synergy with B. infantis, promotes the biosynthesis of shortchain fatty acids, enhancing intestinal barrier function and suppressing local inflammation [26]. 3'-Sialyllactose may



ameliorate liver diseases via mechanisms mediated by the gut-liver axis. An increase in sialylation modification is closely associated with the metastatic potential of HCC cells and the establishment of an immunosuppressive microenvironment.

This study found that compared with healthy people, patients with hepatitis B-related liver cancer had significant changes in metabolic pathways such as cofactors and vitamins, carbohydrates, and amino acids. The seven metabolic pathways enriched in this study encompass several hallmark features of metabolic reprogramming in liver cancer, collectively reflecting the adaptive alterations in energy supply, biosynthesis, and redox balance in liver cancer cells. HBV infection is a major risk factor for liver cirrhosis and HCC [27], significantly altering the metabolic state of hepatocytes. Pantothenate and CoA biosynthesis represent the most significantly altered metabolic pathways in this study. Pantothenate is a precursor for CoA synthesis, and its deficiency can impair CoA production, disrupting the formation of acetyl-CoA and its mediation of various core metabolic processes. Acetyl-CoA can regulate the expression of HCC tumor-initiating cells associated genes through epigenetic mechanisms, such as enhanced acetylation of Histone H3 Lysine 27 (H3K27), thereby promoting the initiation and progression of HCC [28]. Its metabolic accumulation further accelerates HCC metastasis [29]. The significant enrichment of this pathway not only reflects severe metabolic dysregulation in hepatitis B-related liver disease but also underscores its critical pathological role in the malignant transformation of hepatocytes and the development of liver cancer.

This study indicates that urinary metabolic profiles can effectively classify HCC patients. The identification of cancer subtypes is a fundamental cornerstone for achieving personalized diagnosis and treatment in cancer patients [30]. The use of metabolism-related genes expression profiles has defined a new classification system for HCC, providing a framework to understand its genetic diversity [31]. Based on Hallmark and KEGG pathways enrichment analyses, two distinct molecular subtypes exhibit significant differences in pathways related to the cell cycle, metabolism, and tumor microenvironment. Our analysis revealed that the C1 subtype was associated with more aggressive clinicopathological features, including higher tumor grade and more advanced T stage, which likely contributed to its significantly poorer survival outcomes compared to the C2 subtype. These findings highlight the crucial prognostic significance of subtyping in HCC and suggest that patients with the C1 subtype may necessitate more intensive management and individualized therapeutic strategies. These findings provide important insights into liver cancer heterogeneity and form an important foundation for developing precision therapeutic strategies.

This study aimed to explore the relationship between the liver cancer immune microenvironment and tumor immune evasion based on urinary metabolic characteristics. This review has shown that HCC tumors exhibit complex interactions within the immune microenvironment [32], as abnormal glucose metabolism enables cancer cells to adapt to microenvironmental changes and evade immune surveillance [33]. Nutrient deficiency and metabolic dysregulation not only accelerate tumor progression but also compromise the functional capacity of immune cells [34]. The metabolism of MDSC can regulate their immunosuppressive functions [35], and the increase in these cells promotes the immune-tolerant tumor microenvironment [36]. The metabolic reprogramming within the tumor immune microenvironment, characterized by nutrient competition between tumor and immune cells, generates immunomodulatory metabolites. These molecules enter circulation and may be renally filtered into urine, offering a rational basis for using urinary metabolites as non-invasive biomarkers of systemic and tumor immune microenvironment-specific metabolic alterations. The metabolic profile of urinary metabolites holds the potential to reflect the immune microenvironment of liver cancer, tumor dynamics, and therapeutic responses, offering new possibilities for the study of disease progression and therapeutic interventions in liver cancer.

Although the metabolic biomarkers and associated regulatory genes identified in this study were initially derived from a hepatitis B-related liver cancer context, their significant prognostic value in the general TCGA-LIHC cohort suggests that their relevance may extend beyond HBVdriven hepatocarcinogenesis, likely reflecting a broader biological mechanism prevalent across HCC populations with diverse etiologies. HBV drives carcinogenesis by disrupting the hepatic immune microenvironment, leading to chronic inflammation and malignant transformation [37]. This is further exemplified by the specific finding that Solute Carrier Family 16 Member 3 (SLC16A3), a marker for immunosuppressive Kupffer cells, is highly expressed in HBV-positive HCC and linked to poor prognosis [38]. Thereby highlighting the significant impact of the distinctive immune microenvironment in HBV-associated HCC on tumor progression and patient outcomes. The presence of HBV DNA is not merely a biomarker of infection but a central driver that shapes the immunosuppressive HCC microenvironment. DNA sensors play a pivotal role in anti-tumor immunity, and alterations in their expression significantly influence the HCC tumor microenvironment, thereby shaping disease progression and patient prognosis [39]. While we recognize that the tumor microenvironment undoubtedly differs between HBV-infected and noninfected individuals, our findings offer only a foundational insight. Therefore, these results must be considered preliminary and require future validation in larger, etiologystratified cohorts to confirm their generalizability and specificity.



### 5. Conclusions

Our study indicates that Suberic acid, 2'-O-methylcytidine, and 3'-Sialyllactose in urine demonstrate good accuracy in distinguishing between hepatitis B-related liver cancer and healthy individuals. Based on the regulatory genes associated with differential metabolites, our research identifies two distinct molecular subtypes of HCC, aiming to advance the development of precision and personalized diagnosis and treatment for PLC. However, this study still has some limitations. Firstly, the sample size is relatively small, and it is necessary to increase the sample size to validate and explore the association between metabolites and PLC, as well as potential biomarkers. Secondly, further validation and optimization of the stability and reliability of the prognostic model are required.

# Availability of Data and Materials

The dataset that used, analyzed, or generated in this research is available from the corresponding author upon reasonable request.

### **Author Contributions**

HW and HL were responsible for experimental design and manuscript writing. MFL and XZ provided guidance on experimental design and manuscript revisions. FL, RZ, MPL participated in the collection of clinical samples and data. YW, FS, YZ conducted the analysis of results and data interpretation. All authors contributed to editorial changes in the manuscript. All authors read and approved the final manuscript. All authors have participated sufficiently in the work and agreed to be accountable for all aspects of the work.

### **Ethics Approval and Consent to Participate**

This study was approved and authorized by the Ethics Committee of the First Affiliated Hospital of Guangxi University of Chinese Medicine (approval No. Z-A 2023-013-01), and was conducted in accordance with the principles of the Declaration of Helsinki. Informed consent was obtained from either the participants or their family members prior to specimen collection.

### Acknowledgment

We sincerely thank the patients for their involvement in this study. We are grateful to Gene Denovo Biotechnology Co., Ltd. (Guangzhou, China) for assisting in the metabolite and bioinformatics analyses.

### **Funding**

This research was funded by Natural Science Foundation of Guangxi, grant number 2025GXNSFDA069035, 2025GXNSFAA069372; Self-funded Scientific Research Project in Western Medicine by the Guangxi Health Commission, grant number Z-A20230917.

### **Conflict of Interest**

The authors declare no conflict of interest. Although we received technical assistance from Gene Denovo Biotechnology Co., Ltd., the judgments in data interpretation and writing were not influenced by this relationship.

### References

- [1] Wang K, Li X, Guo S, Chen J, Lv Y, Guo Z, et al. Metabolic reprogramming of glucose: the metabolic basis for the occurrence and development of hepatocellular carcinoma. Frontiers in Oncology. 2025; 15: 1545086. https://doi.org/10.3389/fonc.2025. 1545086.
- [2] Han W, Wang B, Yong X, Zhang Y, Shao M, Wang C. Indolent T-lymphoblastic proliferation with fibrolamellar hepatocellular carcinoma developed after colorectal adenocarcinoma: a case report. Pathology Oncology Research: POR. 2023; 29: 1611151. https://doi.org/10.3389/pore.2023.1611151.
- [3] Tümen D, Heumann P, Gülow K, Demirci CN, Cosma LS, Müller M, et al. Pathogenesis and Current Treatment Strategies of Hepatocellular Carcinoma. Biomedicines. 2022; 10: 3202. https://doi.org/10.3390/biomedicines10123202.
- [4] Rao H, An X, Qu X, Yu J, Xie J, Ke J, *et al.* SGLT2i delays c-Myc-induced HCC progression via targeting mTOR. Biochimica et Biophysica Acta. Molecular Basis of Disease. 2025; 1871: 167805. https://doi.org/10.1016/j.bbadis.2025.167805.
- [5] Yao X, Ling X, Zhu Z, Cao X, Tang S. Temporal trends of liver cancer burden, comparative analysis of risk factors and trend forecasts to 2024 in China, USA, the Republic of Korea, and Mongolia: an analysis based on multiple data sources from Global Burden of Disease 2019, the Global Cancer Observatory, and Cancer Incidence in Five Continents. Journal of Global Health. 2025; 15: 04040. https://doi.org/10.7189/jogh .15.04040.
- [6] Zhao YQ, Cong WM. Advances in the diagnostic pathological features of precancerous lesions of hepatocellular carcinoma. Zhonghua Gan Zang Bing Za Zhi. 2019; 27: 491–493. https://doi.org/10.3760/cma.j.issn.1007-3418.2019.07.004. (In Chinese)
- [7] Attia AM, Rezaee-Zavareh MS, Hwang SY, Kim N, Adetyan H, Yalda T, et al. Novel Biomarkers for Early Detection of Hepatocellular Carcinoma. Diagnostics (Basel, Switzerland). 2024; 14: 2278. https://doi.org/10.3390/diagnostics14202278.
- [8] Gao Y. On Research and Translation of Urinary Biomarkers. Advances in Experimental Medicine and Biology. 2021; 1306: 101–108. https://doi.org/10.1007/978-3-030-63908-2 7.
- [9] Xie XF, Sun Y, Zhao XH. Urine metabolomics study of hepatocellular carcinoma. Zhonghua Zhong Liu Za Zhi. 2022; 44: 252– 259. https://doi.org/10.3760/cma.j.cn112152-20200825-00765. (In Chinese)
- [10] Haghir-Sharif-Zamini Y, Khosravi A, Hassan M, Zarrabi A, Vosough M. c-FLIP/Ku70 complex; A potential molecular target for apoptosis induction in hepatocellular carcinoma. Archives of Biochemistry and Biophysics. 2025; 765: 110306. https://doi.org/10.1016/j.abb.2025.110306.
- [11] Lei YR, He XL, Li J, Mo CF. Drug Resistance in Hepatocellular Carcinoma: Theoretical Basis and Therapeutic Aspects. Frontiers in Bioscience (Landmark edition). 2024; 29: 52. https: //doi.org/10.31083/j.fbl2902052.
- [12] Zhou J, Chen TW, Guo DJ. Research progress and prospects of the application of radiographic imaging in the precise diagnosis and treatment of hepatocellular carcinoma. Zhonghua Gan Zang Bing Za Zhi. 2024; 32: 673–678. https://doi.org/10.3760/cma.j. cn501113-20240529-00275. (In Chinese)
- [13] Yang G, Liu R, Rezaei S, Liu X, Wan YJY. Uncovering the Gut-Liver Axis Biomarkers for Predicting Metabolic Burden



- in Mice. Nutrients. 2023; 15: 3406. https://doi.org/10.3390/nu 15153406
- [14] Kang W, Choi D, Son B, Park S, Park T. Activation of OR10A3 by Suberic Acid Promotes Collagen Synthesis in UVB-Irradiated Dermal Fibroblasts via the cAMP-Akt Pathway. Cells. 2022; 11: 3961. https://doi.org/10.3390/cells11243961.
- [15] Wang G, Li J, Bojmar L, Chen H, Li Z, Tobias GC, et al. Tumour extracellular vesicles and particles induce liver metabolic dysfunction. Nature. 2023; 618: 374–382. https://doi.org/10.1038/ s41586-023-06114-4.
- [16] Alannan M, Fatrouni H, Trézéguet V, Dittrich-Domergue F, Moreau P, Siegfried G, et al. Targeting PCSK9 in Liver Cancer Cells Triggers Metabolic Exhaustion and Cell Death by Ferroptosis. Cells. 2022; 12: 62. https://doi.org/10.3390/cell s12010062.
- [17] Carroll SS, Tomassini JE, Bosserman M, Getty K, Stahlhut MW, Eldrup AB, et al. Inhibition of hepatitis C virus RNA replication by 2'-modified nucleoside analogs. The Journal of Biological Chemistry. 2003; 278: 11979–11984. https://doi.org/10.1074/jb c.M210914200.
- [18] Fang Z, Hu Y, Chen J, Xu K, Wang K, Zheng S, et al. Mass Spectrometry-Based Targeted Serum Monomethylated Ribonucleosides Profiling for Early Detection of Breast Cancer. Frontiers in Molecular Biosciences. 2021; 8: 741603. https://doi.or g/10.3389/fmolb.2021.741603.
- [19] Fang Z, Hu Y, Hong X, Zhang X, Pan T, Pan C, et al. Simultaneous Determination of Methylated Nucleosides by HILIC-MS/MS Revealed Their Alterations in Urine from Breast Cancer Patients. Metabolites. 2022; 12: 973. https://doi.org/10.3390/metabo12100973.
- [20] Neef SK, Janssen N, Winter S, Wallisch SK, Hofmann U, Dahlke MH, et al. Metabolic Drug Response Phenotyping in Colorectal Cancer Organoids by LC-QTOF-MS. Metabolites. 2020; 10: 494. https://doi.org/10.3390/metabo10120494.
- [21] Kogaki T, Ohshio I, Ura H, Iyama S, Kitae K, Morie T, et al. Development of a highly sensitive method for the quantitative analysis of modified nucleosides using UHPLC-UniSpray-MS/MS. Journal of Pharmaceutical and Biomedical Analysis. 2021; 197: 113943. https://doi.org/10.1016/j.jpba.2021.113943.
- [22] Lv X, Chen X, Liu Y, Yuan L, Wu J, Yao J. Efficient Production of 3'-Sialyllactose Using *Escherichia coli*. Journal of Agricultural and Food Chemistry. 2024; 72: 27314–27325. https://doi.org/10.1021/acs.jafc.4c08703.
- [23] Pessentheiner AR, Spann NJ, Autran CA, Oh TG, Grunddal KV, Coker JK, et al. The human milk oligosaccharide 3'sialyllactose reduces low-grade inflammation and atherosclerosis development in mice. JCI Insight. 2024; 9: e181329. https://doi.org/10. 1172/jci.insight.181329.
- [24] Jin Y, Jeon H, Le Lam Nguyen T, Kim L, Heo KS. Human milk oligosaccharides 3'-sialyllactose and 6'-sialyllactose attenuate LPS-induced lung injury by inhibiting STAT1 and NF-κB signaling pathways. Archives of Pharmacal Research. 2023; 46: 897–906. https://doi.org/10.1007/s12272-023-01470-1.
- [25] Eom HY, Jang SI, Lee JH. Development and Validation of a Bioanalytical Method for 3'- and 6'-Sialyllactose in Minipig Liver and Kidney Using Liquid Chromatography-Tandem Mass Spectrometry and Its Application to Analysis of Tissue Distribution. Molecules. 2020; 25: 5721. https://doi.org/10.3390/mo lecules25235721.
- [26] Yang M, Jiang Z, Zhou L, Chen N, He H, Li W, et al. 3'-Sialyllactose and B. infantis synergistically alleviate gut inflam-

- mation and barrier dysfunction by enriching cross-feeding bacteria for short-chain fatty acid biosynthesis. Gut Microbes. 2025; 17: 2486512. https://doi.org/10.1080/19490976.2025.2486512.
- [27] Wang Y, Wang H, Wei S, Gao Z, Gao H, Wang X, et al. Metabolomic comparative study in patients with liver cirrhosis and hepatocellular carcinoma related to hepatitis B virus infection. European Journal of Gastroenterology & Hepatology. 2025; 37: 1040–1048. https://doi.org/10.1097/MEG.00000000000003021.
- [28] Sun T, Xu C, Song Q, Yang X, An G, Sun G, et al. SIRT4 Controls Acetyl-CoA Synthesis to Promote Stemness and Invasiveness of Hepatocellular Carcinoma through Deacetylating MCCC2. International Journal of Biological Sciences. 2025; 21: 2973–2990. https://doi.org/10.7150/ijbs.99004.
- [29] Pan JJ, Xie SZ, Zheng X, Xu JF, Xu H, Yin RQ, et al. Acetyl-CoA metabolic accumulation promotes hepatocellular carcinoma metastasis via enhancing CXCL1-dependent infiltration of tumor-associated neutrophils. Cancer Letters. 2024; 592: 216903. https://doi.org/10.1016/j.canlet.2024.216903.
- [30] Shi X, Liang C, Wang H. Multiview Robust Graph-Based Clustering for Cancer Subtype Identification. IEEE/ACM Transactions on Computational Biology and Bioinformatics. 2023; 20: 544–556. https://doi.org/10.1109/TCBB.2022.3143897.
- [31] Yang C, Huang X, Liu Z, Qin W, Wang C. Metabolism-associated molecular classification of hepatocellular carcinoma. Molecular Oncology. 2020; 14: 896–913. https://doi.org/10.1002/1878-0261.12639.
- [32] Donne R, Lujambio A. The liver cancer immune microenvironment: Therapeutic implications for hepatocellular carcinoma. Hepatology. 2023; 77: 1773–1796. https://doi.org/10.1002/hep. 32740.
- [33] Zhang Q, Liu J, Lin H, Lin B, Zhu M, Li M. Glucose metabolism reprogramming promotes immune escape of hepatocellular carcinoma cells. Exploration of Targeted Anti-tumor Therapy. 2023; 4: 519–536. https://doi.org/10.37349/etat.2023.00149.
- [34] Xu Y, He L, Fu Q, Hu J. Metabolic Reprogramming in the Tumor Microenvironment With Immunocytes and Immune Checkpoints. Frontiers in Oncology. 2021; 11: 759015. https://doi.org/10.3389/fonc.2021.759015.
- [35] Goldmann O, Medina E. Metabolic pathways fueling the suppressive activity of myeloid-derived suppressor cells. Frontiers in Immunology. 2024; 15: 1461455. https://doi.org/10.3389/fimmu.2024.1461455.
- [36] Kapor S, Radojković M, Santibanez JF. Myeloid-derived suppressor cells: Implication in myeloid malignancies and immunotherapy. Acta Histochemica. 2024; 126: 152183. https://doi.org/10.1016/j.acthis.2024.152183.
- [37] Chiriva-Internati M, Grizzi F, Monari MN, Taverna G, Figueroa JA, Daoyan W, et al. Immunomodulatory role of vitamin D and emerging immunotherapies in hepatocellular carcinoma. Frontiers in Nutrition. 2025; 12: 1611829. https://doi.org/10.3389/fnut.2025.1611829.
- [38] Zhang J, Pan Y, Zhao Z, Chen B, Fan W, Zhao S, et al. SLC16A3 as an immunosuppressive Kupffer cell marker predicts poor prognosis in HBV-positive hepatocellular carcinoma. Journal of Translational Medicine. 2025; 23: 988. https://doi.org/10.1186/ s12967-025-06861-0.
- [39] Lin HS, Pang WP, Yuan H, Kong YZ, Long FL, Zhang RZ, et al. Molecular subtypes based on DNA sensors predict prognosis and tumor immunophenotype in hepatocellular carcinoma. Aging. 2023; 15: 6798–6821. https://doi.org/10.18632/aging. 204870.

